Regular Article

PHYSICAL CHEMISTRY RESEARCH
Published by the
Iranian Chemical Society
www.physchemres.org
info@physchemres.org

Phys. Chem. Res., Vol. 6, No. 1, 115-132, March 2018
DOI: 10.22036/pcr.2017.96386.1411

DFT Study of N-hydroxyurea Adsorption Behavior onto Pristine and Iron-doped Single-walled Carbon Nanotube

M. Hesabi and R. Behjatmanesh-Ardakani*

Department of chemistry, Payame Noor University, P.O. Box: 19395-3697, Tehran, Iran

(Received 26 August 2017, Accepted 14 October 2017)

The interactions between N-hydroxyurea (NHU) as anticancer drug and SWCNTs (pure and Fe-doped) were investigated with density functional theory. In this study, large long-range corrected CAM-B3LYP and B3LYP were employed to investigate the stability of the different NHU-CNT and NHU/Fe-CNT complexes in the gas phase and solution (water). The presence of an iron atom would create the suitable space on the nanotube surface for the adsorption between drug and nanotubes. The results revealed that the adsorption of drugs on the outer surface of both nanotubes was energetically favorable and the reactivity of Fe-doped complexes increased compared to pristine nanotubes. Results indicated that adsorption is dependent on the sites of the drug. NBO, QTAIM and NCI-RDG analyses were applied for further understanding of the adsorption process. The data suggested that the doping of iron atom increases the adsorption ability.

Keywords: Density functional theory, Fe-doped nanotube, Anti-cancer drug, Non-covalent interaction

INTRODUCTION

N-hydroxyurea (Hydrea) is widely employed for the cure of many neoplastic diseases, including chronic myelogneous leukemia, head and neck cancer, sickle cell anemia and polycythemia vera [1-2]. It also treats cancer by slowing the growth of cancer cells in patients. NHU treats sickle cell anemia by helping to reduce and prevent formation of sickle-shaped red blood cells [3]. In addition to its needed effects, some side effects may be caused by NHU, such as drowsiness, nausea, bone marrow toxicity, diarrhea and vomiting, constipation, mucositis, anorexia, stomatitis, abnormal liver enzymes, creatinine and blood urea nitrogen [4]. Side effects may occur when they interact in the incorrect tissue or with unsuitable target.

In order to minimize unwanted effects and toxicity of drugs, an effective method is to send chemical drugs to the target tissues. Drug delivery technologies promote adsorption efficiency and distribution for the benefit of improving product efficacy and safety. In order to attain efficient targeted delivery, the designed systems must active in the target regions of the body and avoid the host's defense mechanisms [5].

Today, carbon nanotubes have received plenty of attention in nanotechnology due to their singular physical properties [6-7]. Carbon nanotubes (CNTs) are promising candidates expected to improve drug delivery because of their exceptional characteristics [8]. The properties of CNTs make them of potential use in many purposes such as improving drug delivery and removing the side effects of drugs. Despite considerable advantages, low solubility of carbon nanotubes is a major setback in the use of nanotubes for biological applications [9-11]. To overcome these problems and improve their activities, researchers have modified nanotubes by doping a heteroatom in the outer surface of nanotubes. Doping as a functionalization method is an effective way for activating the nanotube surface and increasing solubility [12-16].

This study evaluates the interactions between pristine/Fe-doped carbon nanotubes and anti-cancer drug N-

*Corresponding author. E-mail: behjatmanesh@pnu.ac.ir

hydroxyurea based on the density functional theory (DFT). For better evaluation, natural bond orbital (NBO), quantum theory of atoms in molecules (QTAIM) and the reduced density gradient (RDG) are used. To study the electronic properties, using Koopmans' theorem [17,18], quantum descriptors are also calculated. The main goal of this work is to investigate the effect of Fe-doped atom on adsorption ability of N-hydroxyurea drug.

COMPUTATIONAL METHODS

The adsorption behavior of N-hydroxyurea on Fe-doped and undoped (6,0) single wall carbon nanotube in gas and aqueous phases were investigated. In order to increase the validity of calculations, in addition to the density functional theory at the B3LYP level by 6-31g(d) basis set [19], long-range corrected Coulomb-Attenuating method (CAM-B3LYP) by 6-311G(d,p) was also used [20,21]. The geometries of all the studied complexes were optimized by the Ultra Fine Grid keyword and the nature of frequency calculation were carried out using Guassian09 package [22]. To estimate the effect of the solvent, the optimized structures were calculated using polarized continuum model (PCM) with the integral-equation formalism with dielectric constant ε = 78.4 for water as a solvent [23]. The adsorption energies of the structures are defined as:

$$\Delta E_{ads}^{ZPE+BSSE} = E_{\frac{CNT}{NHU}}^{ZPE} - \left(E_{CNT}^{ZPE} + E_{NHU}^{ZPE}\right) + BSSE \quad (1)$$

where $E_{CNT/NHU}^{ZPE}$ is the total energy of the complex between drug and carbon nanotube, and E_{CNT}^{ZPE} and E_{NHU}^{ZPE} are the energies of the nanotube and drug, respectively.

The adsorption energies were corrected by zero-point energy (ZPE) corrections and the basis set superposition error (BSSE) corrections by the counterpoise method[24].

According to Jank's and Parr's theorem [25-26] using the energies of the highest occupied molecular orbital (HOMO) and the lowest unoccupied molecular orbital (LUMO) from the density functional theory, energy gap (E_{H-L}), chemical potential (μ), chemical hardness (η) and global electrophilicity index (ω) were calculated at B3LYP/6-31G(d). These parameters are calculated as follows:

$$\Delta E_{H-L} = E_{LUMO} - E_{HOMO} \quad (2)$$

$$\mu = -\chi = (E_{LUMO} + E_{HOMO})/2 \quad (3)$$

$$\eta = (E_{LUMO} - E_{HOMO})/2 \quad (4)$$

$$\omega = \mu^2/2\eta \quad (5)$$

QTAIM analysis using AIM2000 program [27] and NBO parameters by natural bond orbital (NBO 6) analysis [28] at the CAM-B3LYP/6-311G(d,p) level of theory were also carried out. The JmolNBO program was used for graphical representation of the NBOs [29] at the same level. To identify the nature of weak interaction, RDG-based NCI surfaces were investigated.

RESULTS AND DISCUSSION

Adsorption Energies and Geometries

The interaction between the pristine/Fe-doped (6,0) single-wall carbon nanotube (SWCNT) with length (11.5 Å) and diameter (4.78 Å) and N-hydroxyurea drug was analyzed in different configurations. Substitution of one carbon atom with iron leads to the considerable changes in the structure of carbon nanotube, owing to the larger bond length of Fe-C (1.83 Å) than C-C (1.42 Å). Therefore, the geometric structures of Fe-CNTs are significantly distorted (Fig. 1). Different geometries have been explored to assess the most stable structure of the Fe-doped and undoped complexes. The adsorption of four sites of NHU including -OH, -NH, -C=O and -NH_2 groups on doped and undoped carbon nanotubes have been investigated. In undoped complexes (C complexes), the formation of a complex between site 3 of the drug and CNT is not energetically favorable. The others are presented in Fig. 1. Four configurations concerning to the doped complexes (D complexes) are shown in Fig. 2. As seen in these figures, for undoped complexes, hydrogen atoms and the doped complexes, oxygen and nitrogen atoms of drug are pointing towards carbon and iron of the nanotube, respectively. The

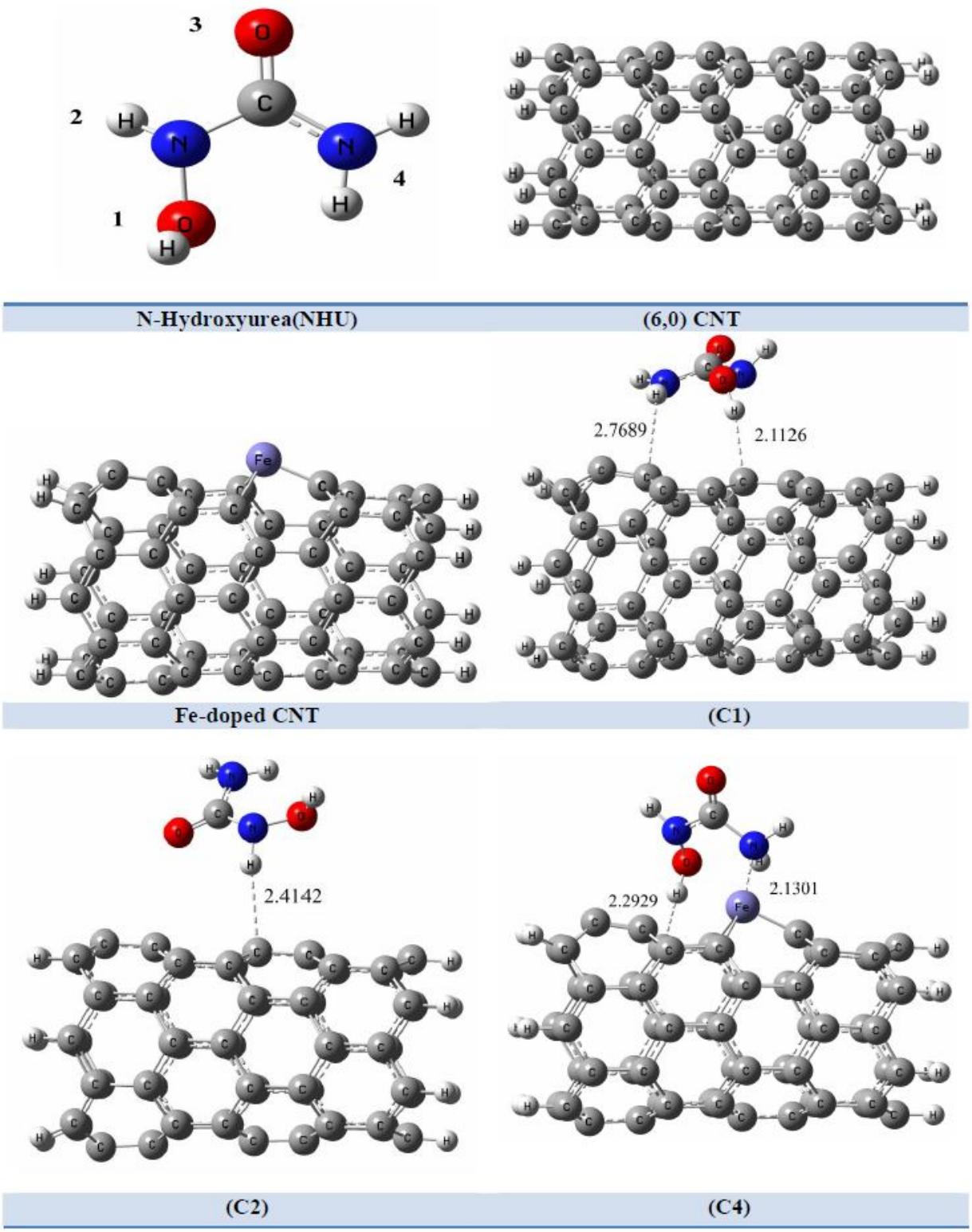

Fig. 1. Optimized geometries of drug, nanotubes and undoped complexes.

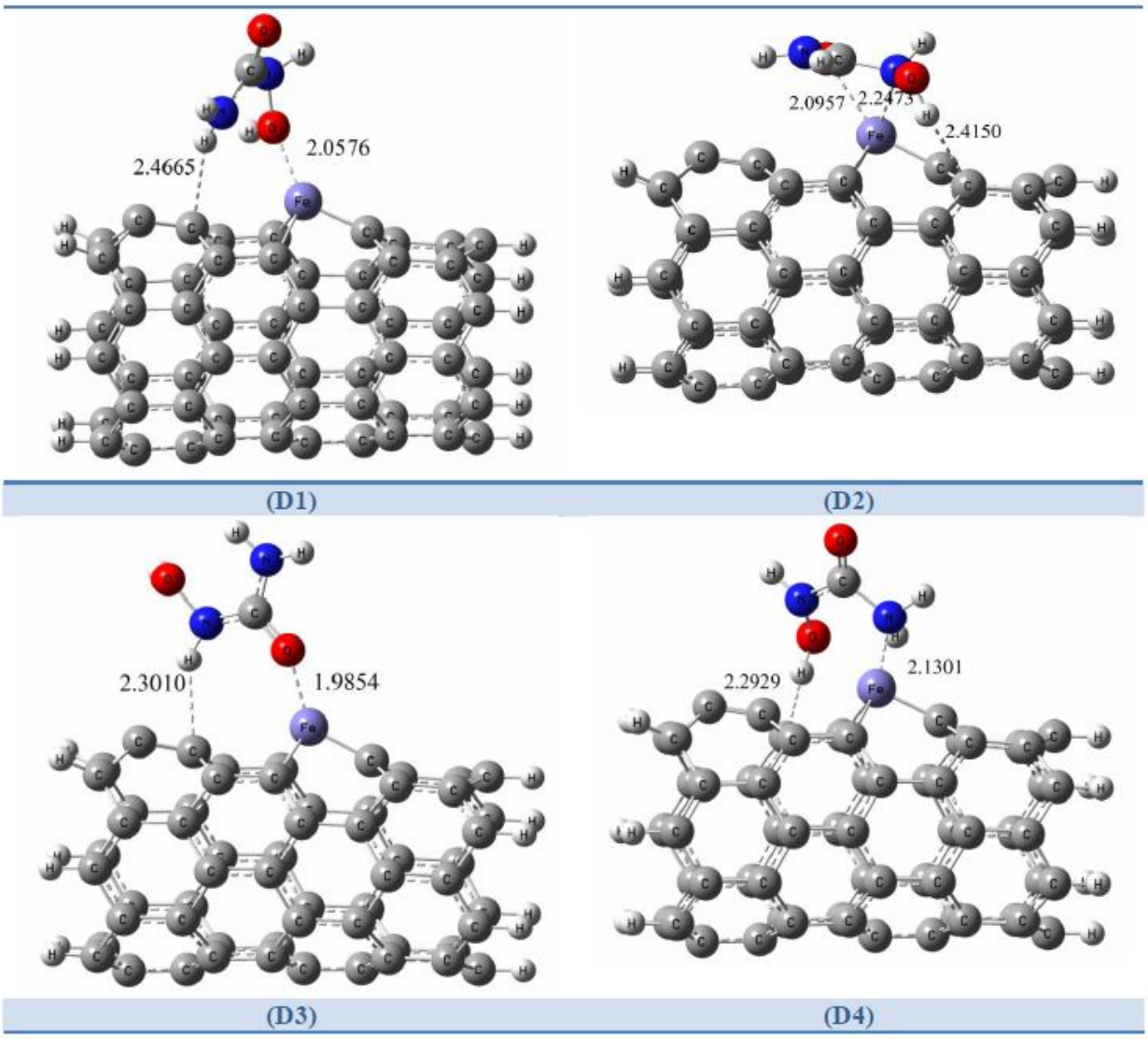

Fig. 2. Optimized geometries of doped complexes.

shortest bond length is related to C1 complex (2.113 Å) and D3 complex (1.985 Å). It is expected that these sites would be the most energetically favorable for the adsorption of NHU molecule.

The average Fe-C bond length of Fe-CNT, average ∠O-Fe-O bond angle and also mulliken, NBO, and AIM charges of iron atom are presented in Table 1. The results clearly show that they change upon adsorption. All Fe-C bonds and charge of Fe atom increase after the adsorption process, whereas, ∠O-Fe-O bond angles decrease. Among all the doped complexes, the Fe atoms of D3, the most stable complex, has the highest charge values.

In order to investigate the effects of the long range interactions, the adsorption energies of complexes in the gas phase and solution (water) were investigated at the B3LYP/6-31G* and CAM-B3LYP/6-311G**levels of theory. The solvation energies and the enthalpy energies were calculated and summarized in Table 2. All the energy

Table 1. Average Equilibrium Bond Lengths (Å), C-Fe-C Angle (°) and Mulliken, AIM and NBO Charges of Fe Atom in Fe-doped Carbon Nanotube and Doped Complexes

	Ave (Fe-C)	Ave ∠C-Fe-C	$q_{Fe}^{Mulliken}$	q_{Fe}^{AIM}	q_{Fe}^{NBO}
Fe-CNT	1.831	94.470	1.049	0.806	0.734
D1	1.844	91.744	1.171	0.874	0.787
D2	1.865	90.358	1.177	0.879	0.788
D3	1.841	90.905	1.242	0.922	0.828
D4	1.847	91.569	1.178	0.861	0.787

Table 2. Calculated Corrected Adsorption Energies, Solvation Energies and Enthalpies for the Studied Complexes (all in kcal mol^{-1})

Complex	$\Delta E_{ads}^{ZPE+BSSE}$		$\Delta E_{Solv.}$		ΔH	
	B3LYP	CAM-B3LYP	B3LYP	CAM-B3LYP	B3LYP	CAM-B3LYP
CNT-1	-1.8937	-11.4928	-8.4022	-20.1767	-3.4111	-12.6274
CNT-2	0.1790	-7.0203	-18.6677	-20.6419	-0.8189	-7.2170
CNT-4	-1.7912	-11.2513	-11.1264	-19.6931	-3.1953	-12.0720
CNT-Fe-1	-10.2523	-14.2012	-18.0814	-20.6306	-19.2351	-21.0028
CNT-Fe-2	-13.0684	-17.4052	-15.3270	-19.8350	-26.5355	-28.0754
CNT-Fe-3	-18.8897	-23.1791	-16.9374	-19.4861	-29.7383	-29.7515
CNT-Fe-4	-12.0967	-16.5078	-18.8202	-21.7576	-22.0582	-24.3405

values were negative, indicating that the complexes are stable. As shown, in all the studied complexes, energies obtained by the CAM-B3LYP method are more negative than those for B3LYP approximately between 3 and 5 kcal mol^{-1} and 7 and 11 kcal mol^{-1} in doped and undoped complexes, respectively. These results are used when considering long-range corrected energy in the CAM-B3LYP method. The most stable configuration for the undoped ones is C1 (with adsorption energy of -11.4928 kcal mol^{-1}), in which NHU interacts with nanotube by the first site (-OH site) and for the doped complexes, it is D3 (with adsorption energy of -23.1791 kcal mol^{-1}), in which NHU interacts with nanotube *via* its third site (-C=O site) which are in line with the results of geometric parameters in Table 1. Negative values of enthalpy indicate that the adsorption process is exothermic, thus, the formation of all complexes is acceptable. The higher values of solvation energy (more negative) indicate that functionalization of

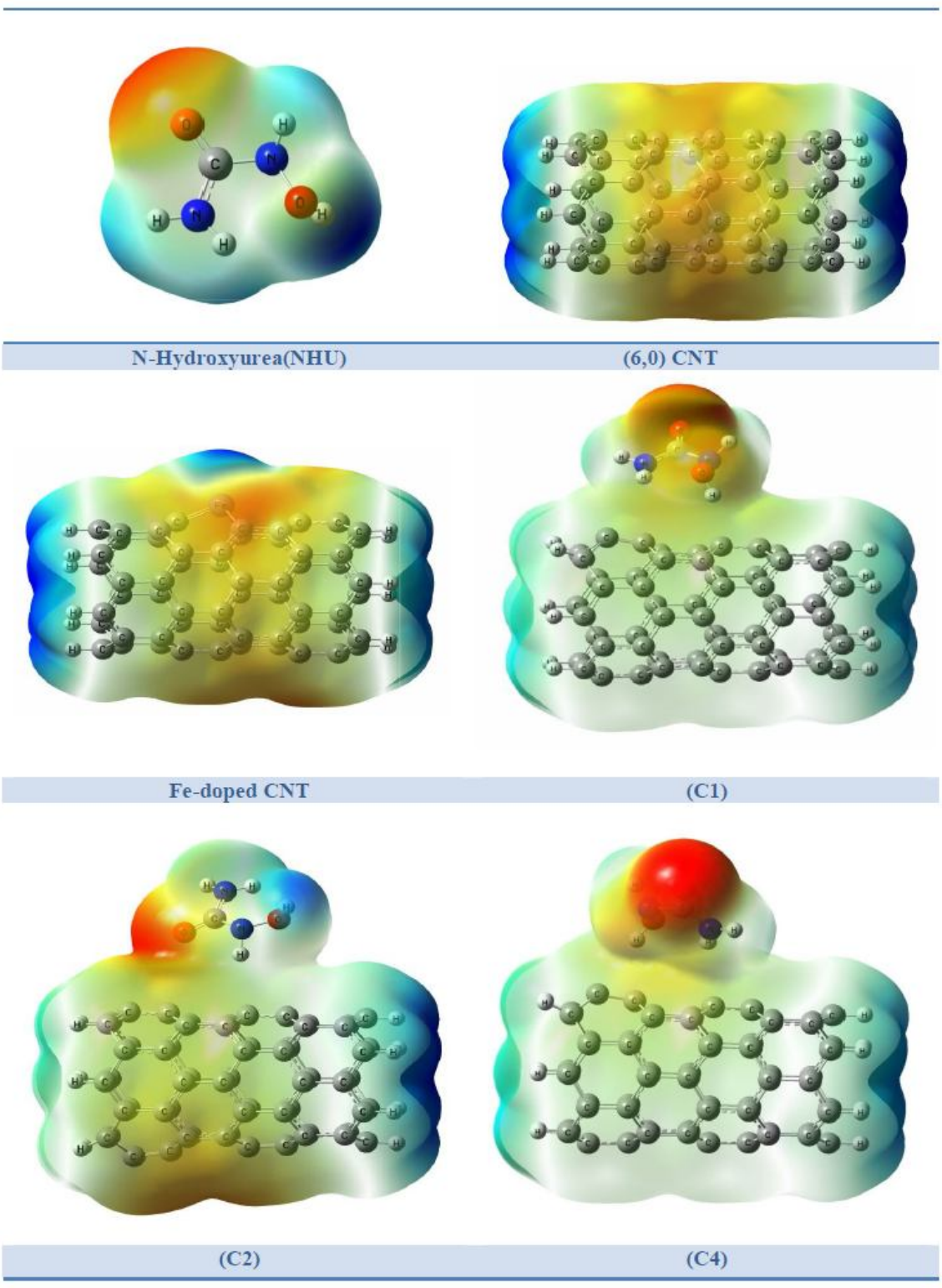

Fig. 3. MEP maps of the considered structures.

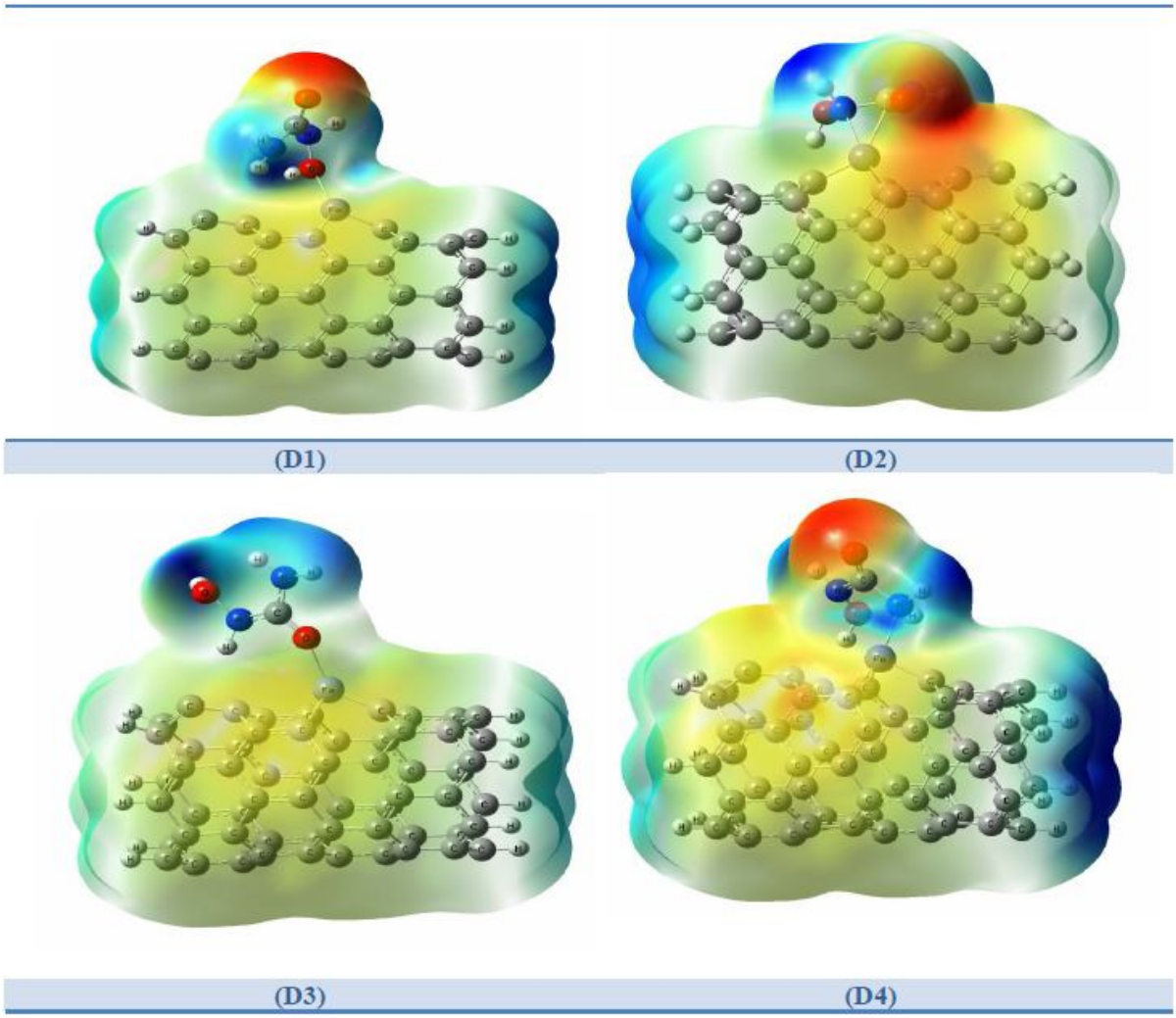

Fig. 3. Continued.

nanotubes by doping Fe atoms can modify their interactions and also enhance the solubility of NHU-nanotubes.

The molecular Electrostatic Potential (MEP)

The MEP is a useful plot to interpret and predict the electrophilic and nucleophilic sites. The different values of the electrostatic potential are represented by various colors. Blue and red colors show the strongest attraction and repulsion, respectively [30]. MEP plots of NHU, CNTs and complexes have been shown in Fig. 3. As seen in Fig. 3, the negative sites are placed on the carbonyl group. The positive sites are over the hydrogen atoms and the region of zero potential are located over the pristine nanotube (green color). It is expected that the electron-rich O atom of drug should interact with the electron poor Fe atom of the nanotube. Figure 3 indicates that after the adsorption process, the drug is more positive, confirming a charge transfer from the drug to the nanotube. On the other hand, after the doping of CNT, the D3 complex becomes more positive. This shows that site 3 of the drug for doped and site1 for undoped complexes are suitable for the adsorption process, and charge transfer takes place between the

Table 3. The reactivity Descriptors of all Structures (all in eV) and Dipole Moment (Debye)

	HOMO	LUMO	ΔE_{H-L}	η	μ	ω	d
NHU	-6.963	0.963	7.926	3.963	-3.000	1.136	1.359
CNT	-3.530	-2.861	0.669	0.335	-3.196	15.245	0.000
CNT-Fe	-3.661	-2.933	0.728	0.364	-3.297	14.932	0.680
CNT-1	-3.701	-2.995	0.706	0.353	-3.212	15.877	2.370
CNT-2	-3.512	-2.841	0.671	0.335	-3.176	15.055	0.861
CNT-4	-3.565	-2.860	0.705	0.353	-3.348	14.613	2.271
CNT-Fe-1	-4.161	-3.116	1.045	0.522	-3.639	12.684	1.352
CNT-Fe-2	-3.982	-2.994	0.988	0.494	-3.488	12.314	2.217
CNT-Fe-3	-3.710	-2.718	0.992	0.496	-3.214	10.413	3.263
CNT-Fe-4	-4.039	-3.002	1.037	0.518	-3.521	11.967	1.918

nanotube and NHU.

Electronic Properties

To compare the electronic changes of CNT and Fe-CNT, the electronic structure descriptors should be computed. The highest occupied molecular orbital (HOMO), the lowest unoccupied molecular orbital (LUMO), the global indices of reactivity, the gap of energy (ΔE_{H-L}), and dipole moment (d) are shown in Table 3. The electrons were transferred from the higher electronic chemical potential (μ) to the lower one when NHU was adsorbed on nanotubes. The chemical potential of both CNT (-3.20 eV) and Fe-CNT (-3.27 eV) are lower than the drug molecule (-3.00 eV), so electrons flow from NHU to CNT and Fe-CNT. The electrophilicity index (ω) exhibited the capability of the drug to accept the electron [31]. The results show that the electrophilicity of Fe-CNT compared to CNT decreases, showing its stability after doping the iron atom. When NHU is adsorbed on the functionalized nanotube, the electronic chemical potential increases and the electrophilicity of complexes decreases. The values of dipole moment increase by functionalization with Fe-doping and also after adsorption of NHU on CNTs, which is the expected parameter for drug delivery in biological nanosystems. The D3 complex with the lowest electrophilicity and the highest electronic chemical potential and dipole moments is the most stable complex.

B3LYP is a credible method for determining the band gap as mentioned in the literature [32,33]. The band gap of the drug is very much higher than that for both CNT and Fe-CNT indicating the increase in electrical conductivities of drug upon complexation. It is observed that the values of ΔE_g of complexes increase compared to those of CNT and Fe-CNT; this can be related to the interaction between the N-hydroxyurea and CNTs.

QTAIM Topological Analysis and RDG-NCI Index

The theory of quantum atoms in molecules defines the chemical bonding and chemical structure of a system based on the topology of the electron density [34]. This theory was introduced by Richard Bader [39]. The values of Laplacian ($\nabla^2\rho$), electron density ρ(r) and other characteristics such as the kinetic energy density (G), potential energy density (V), the total energy density (H) and the ratio of $|V|/G$ and eigen values of hessian matrix are given in Table 4. The molecular graphs are shown in Figs. 4 and 5, where the positions of all bonds critical points (BCPs) between the drug and nanotubes are indicated. The total energy density helps to characterize the nature of bonds between pairs of interacting

Table 4. QTAIM Topological Parameters for Studied Complexes

Complex	BD (Å)	ρ (e/a_0^3)	$\nabla^2\rho$ (e/a_0^5)	λ_2	V(r)	G(r)	H(r)	|V(r)|/G(r)
C1								
C41…H81	2.1126	0.02186	0.0521	-0.0232	-0.0124	0.0127	0.0003	0.9780
C43…H80	2.7689	0.0065	0.0175	-0.0029	-0.0029	0.0036	0.0008	0.7949
C2								
C41…H78	2.4142	0.0115	0.0304	-0.0098	-0.0054	0.0065	0.0011	0.8266
C4								
C38…H81	2.3250	0.0151	0.0394	-0.0092	-0.0068	0.0083	0.0016	0.8135
C40…H80	2.6681	0.0077	0.0210	-0.0046	-0.0036	0.0045	0.0009	0.8197
D1								
Fe72…O77	2.0575	0.0653	0.3843	-0.0661	-0.0975	0.0968	-0.0007	1.0075
C38…H80	2.4665	0.0107	0.0284	-0.0066	-0.0047	0.0059	0.0012	0.7966
D2								
Fe72…N73	2.0957	0.0655	0.3542	-0.0432	-0.1000	0.0943	-0.0057	1.0606
Fe72…O75	2.2473	0.0445	0.2278	-0.0094	-0.0564	0.0566	0.0003	0.9951
C52…H81	2.4150	0.0121	0.0321	-0.0091	-0.0060	0.0070	0.0010	0.8571
D3								
Fe72…O75	1.9854	0.0775	0.4563	-0.1164	-0.1214	0.1177	-0.0037	1.0314
C38…H78	2.3010	0.0175	0.0429	-0.0100	-0.0075	0.0091	0.0016	0.8242
D4								
Fe72…N76	2.1301	0.0630	0.2889	-0.0529	-0.0858	0.0790	-0.0068	1.0858
C39…H81	2.2929	0.0177	0.0177	-0.0077	-0.0087	0.0104	0.0017	0.8375

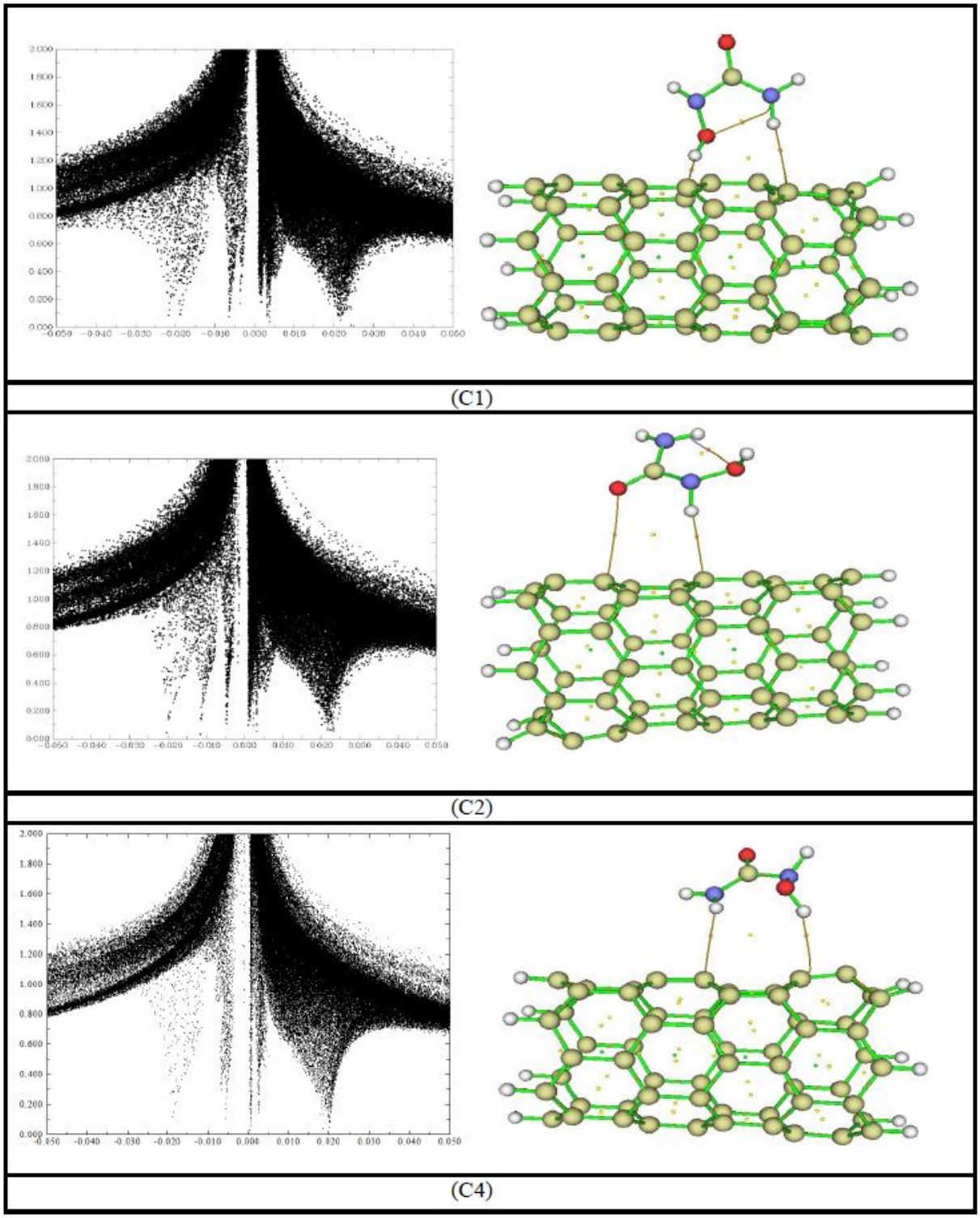

Fig. 4. The obtained AIM molecular graphs (Right) and RDG plots (Left) of the undoped complexes. In RDG plots, x and y axis are sign (λ2) ρ and RDG respectively.

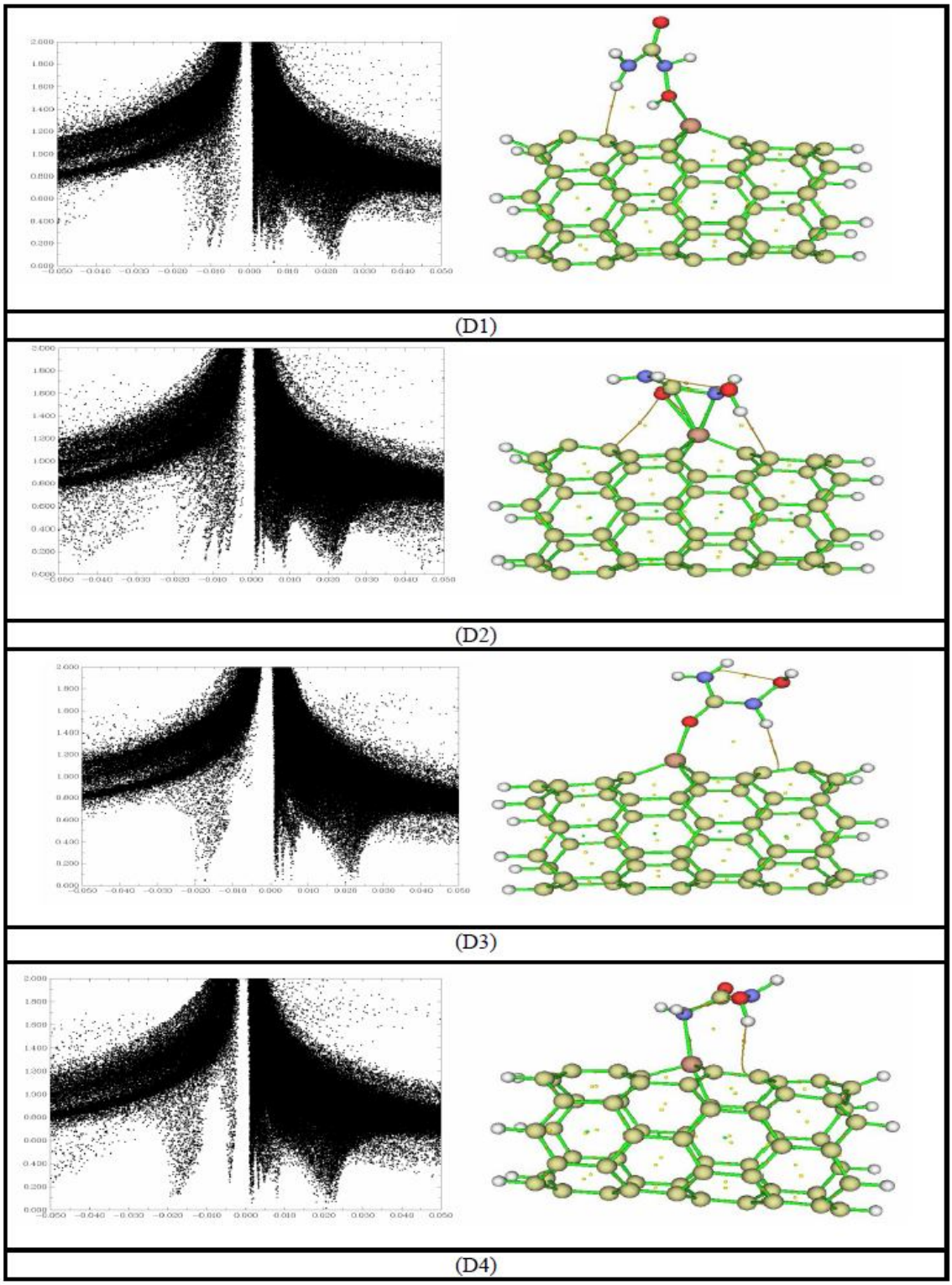

Fig. 5. The obtained AIM molecular graphs (Right) and RDG plots (Left) of the doped complexes. In RDG plots, x and y axis are sign (λ2) ρ and RDG respectively.

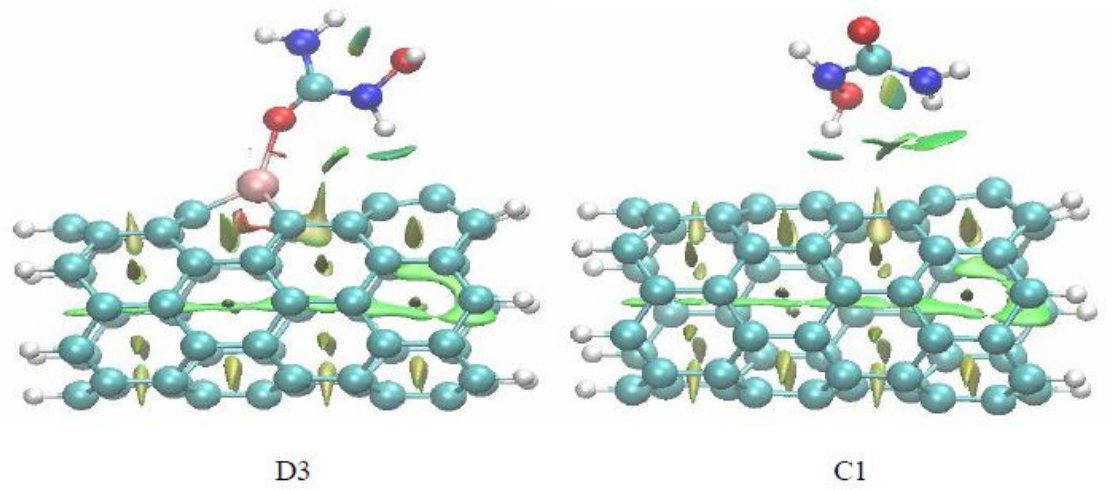

Fig. 6. NCI surface Gradient for D3 and C1 complexes and isosurfaces (0.5 a.u.). Iron, carbon, hydrogen, oxygen, and nitrogen atoms are shown in pink,light blue, white, red, dark blue, respectively.

atoms. It is the sum of G and V parameters. The more negative Hamiltonian at BCPs the more covalent is the bond. The large and positive ρ(r) and $\nabla^2\rho$ values can make a chemical bond stronger than the others. Ionic interaction is related to the high electron density, while if the charge density is low the nature of interactions is of the weak Vander Waals forces, and if the sign of ρ(r) and H opposed each other, the bond is partially covalent and partially electrostatic [35]. Finally, the $|V|/G$ ratio is a suitable parameter to classify the interatomic interactions. Electrostatic interactions are associated with $|V|/G \leq 1$, intermediate interactions $1 < |V|/G > 2$, and the shared interactions $|V|/G > 2$ [36]. It is obvious from Table 4 that in all of the Fe-doped complexes, there are both cases of $H > 0$ and $H < 0$; thus, both characters of being partially covalent and partially electrostatic are seen. The $|V|/G$ values confirmed these interactions too. Results show that the D3 complex with the lowest bond distance (1.985 Å) has the largest ρ(r) and $\nabla^2\rho$. In undoped complexes, positive H and $\nabla^2\rho$, small ρ(r) value and $|V|/G < 1$ confirm the electrostatic interaction.

To evaluate and characterize the nature of the weak interactions the reduced density gradient (*RDG or s*) for the studied complexes was applied. The $s(\rho)$ is defined as:

$$s(\rho) = \frac{1}{2(3\pi^2)^{1/3}} \frac{|\nabla\rho(r)|}{\rho(r)^{4/3}} \quad (6)$$

The sign $(\lambda 2)\rho$ parameter (product between sign ((2) and ρ(r)) has been proposed as a tool to distinguish the attraction and repulsion of interactions. The second lowest eigen values of electron density hessian matrix ((2) values are listed in Table 4. The scatter graphs of RDG versus sign $(\lambda 2)\rho$ were obtained with the MultiWFN program [37] and VMD program [38]. The strength of the weak interaction based on the peaks that appear at low and high densities is identified. The hydrogen bonding or dipole-dipole interaction (attractive interaction) regions have $\rho > 0$ and $\lambda_2 < 0$ while $\rho > 0$ and $\lambda_2 > 0$ is related to repulsion interaction regions [39].

It can be seen in Figs. 4, and 5. In undoped complexes, there are several spikes about $\rho = 0$ due to van der Waals forces and the effect of attractive interactions at high density region can be observed clearly. In doped complexes, the D3 complex, the highest stable complex does not have any spike near the zero field of the x-axis verifying the presence of an attractive interaction. The vdW interactions have been clearly shown at the isosurface 0.5 a.u. in other complexes. The graphical presentations of variable regions of the stable complexes (D3 and C1) are identified using NCIPLOT [40]

Table 5. Calculated Natural Hybrids, Occupancies, and the Second-order Perturbation Energy $E^{(2)}$ at CAM-B3LYP/6-311G(d,p)

Complex	Donor			Acceptor			$E^{(2)}$
	Type	Hybrid	Occupancy	Type	Hybrid	Occupancy	(kcal mol^{-1})
D1	LP(1) O77	$SP^{99.99}\ d^{0.05}$	1.9662	σ* C41…Fe72	$Sd^{3.31}$	0.2492	1.27
				σ* C50…Fe72	$Sd^{1.80}$	0.1363	1.33
	LP(2) O77	$SP^{0.88}$	1.9254	σ* C40…Fe72	$Sd^{1.90}$	0.0866	1.59
				σ* C41…Fe72	$Sd^{3.31}$	0.2492	5.84
				π* C41…Fe72	$SP^{22.95}d^{0.01}$	0.4113	9.84
				σ* C50…Fe72	$Sd^{1.80}$	0.1363	17.74
D2	LP(1) N73	$SP^{3.97}$	1.7964	σ* C40…Fe72	$Sd^{1.75}$	0.1774	40.34
	LP(1) O75	$SP^{0.7}$	1.9666	σ* C40…Fe72	$Sd^{1.75}$	0.1774	1.91
				σ* C41…Fe72	$Sd^{2.38}$	0.1427	4.22
				σ* C50…Fe72	$Sd^{1.99}$	0.1023	3.14
	LP(2) O75	$SP^{99.99}\ d^{0.11}$	1.8374	σ* C41…Fe72	$Sd^{2.38}$	0.1427	4.54
				σ* C50…Fe72	$Sd^{1.99}$	0.1023	3.12
	LP(3) O75	$SP^{99.99}\ d^{0.54}$	1.5603	σ* C41…Fe72	$Sd^{2.38}$	0.1427	8.84
D3	LP(1) O75	$SP^{1.08}$	1.9206	σ* C40…Fe72	$Sd^{1.79}$	0.1171	12.11
				σ* C41…Fe72	$Sd^{2.87}$	0.2163	3.56
				π* C41…Fe72	$SP^{37.85}\ d^{0.01}$	0.3923	7.67
				σ* C50…Fe72	$Sd^{1.82}$	0.1160	7.43
	LP(2) O75	$SP^{7.76}$	1.8574	σ* C40…Fe72	$Sd^{1.79}$	0.1171	4.19
				σ* C41…Fe72	$Sd^{2.87}$	0.2163	11.92
				π* C41…Fe72	$SP^{37.85}\ d^{0.01}$	0.3923	14.27
				σ* C50…Fe72	$Sd^{1.82}$	0.1160	5.10
	LP(3) O75	SP	1.6711	σ* C50…Fe72	$Sd^{1.82}$	0.1160	2.65
D4	LP(1)N76	$SP^{4.75}$	1.8016	LV(1)C41	$SP^{75.68}d^{0.03}$	0.8141	2.96
				σ* C40…Fe72	Sd^{2}	0.0836	1.16
				σ* C50…Fe72	$Sd^{1.84}$	0.1738	42.98
C1	πC39…C41	$SP^{99.99}\ d^{0.06}$	1.7824	σ* O77…H81	S	0.02032	5.60
	σ O77…H81	$SP^{2.98}$	1.9900	π*C39…C41	$SP^{99.99}\ d^{4.94}$	0.3814	1.45
C2	πC36…C41	$SP^{99.99}\ d^{0.14}$	1.5930	σ* N73…H78	S	0.0212	1.84
C4	πC36…C38	$SP^{99.99}\ d^{0.18}$	1.8767	σ* O77…H81	S	0.0155	4.11

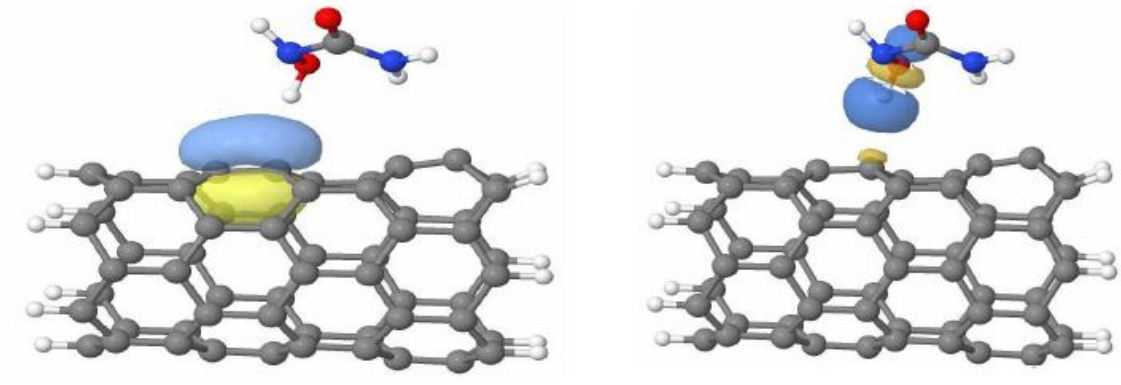

(C1) πC39-C41 [HOMO]→ σ^*O77-H81: 5.60 kcal mol^{-1}

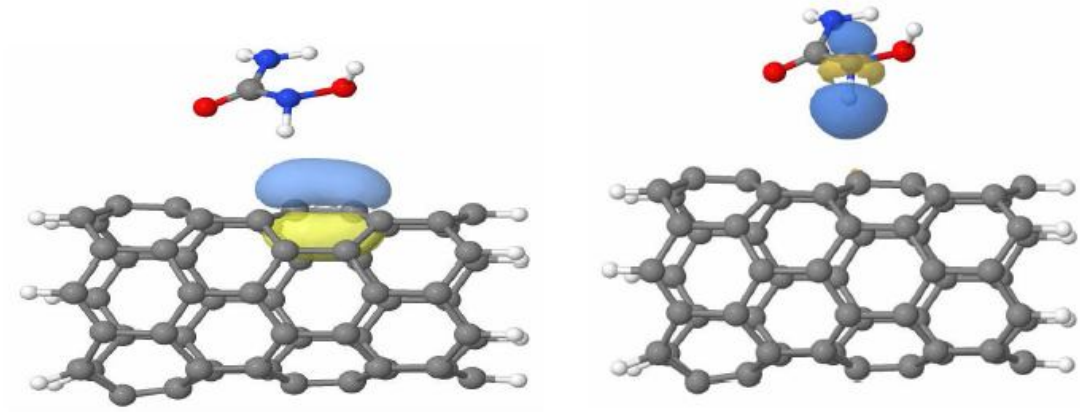

(C2) πC39-C41 [HOMO]→ σ^*N73-H78: 1.84 kcal mol^{-1}

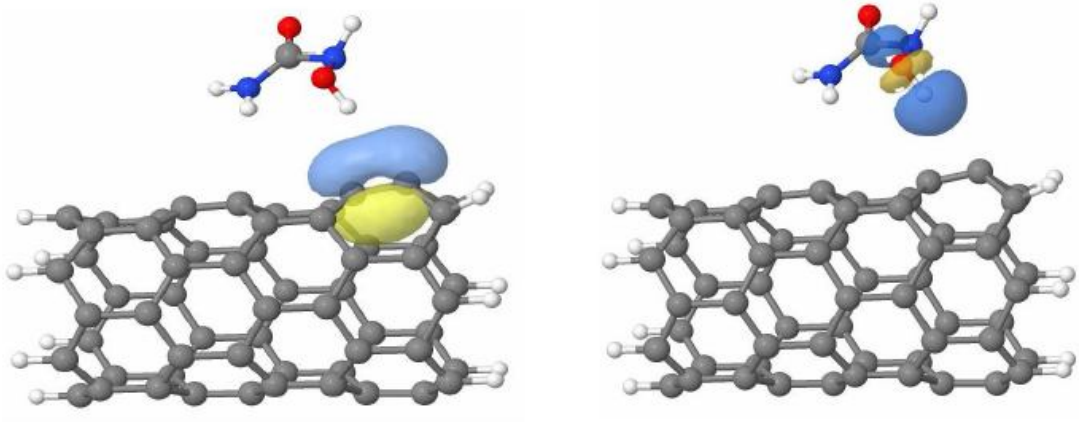

(C4) πC36-C38 [HOMO]→ σ^*O77-H81: 4.11 kcal mol^{-1}

Fig. 7. Selected orbital interaction for undoped complexes

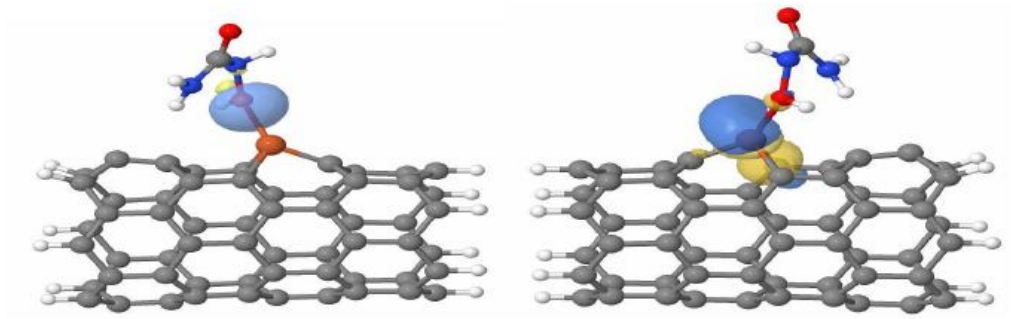

(D1) LP(2)O77 [HOMO]→ σ^*C50-Fe72: 17.74 kcal mol^{-1}

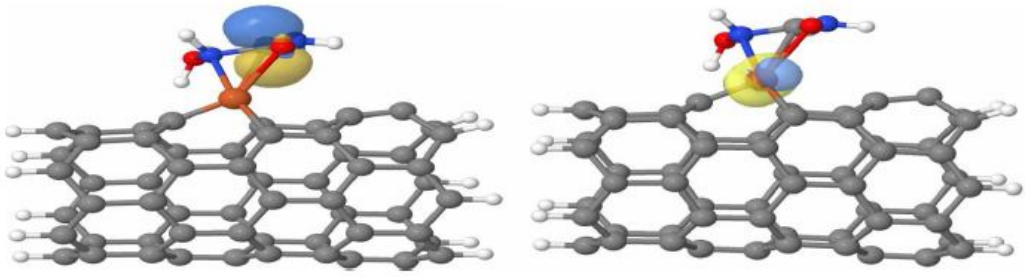

(D2) LP(1)N73 [HOMO]→ σ^*C40-Fe72: 40.34 kcal mol^{-1}

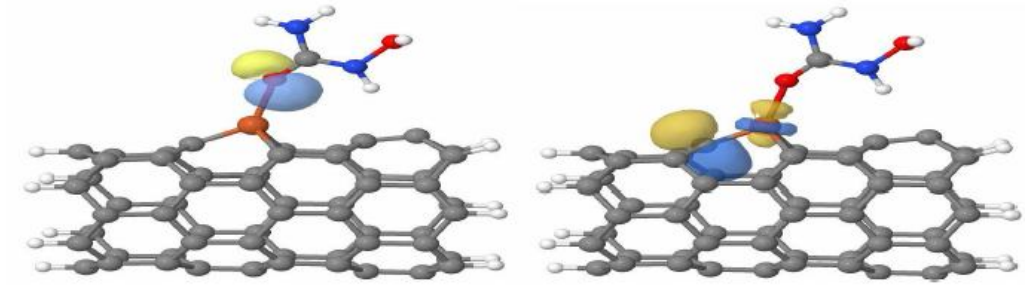

(D3) LP(2)O75 [HOMO]→ π^*C41-Fe72: 14.27 kcal mol^{-1}

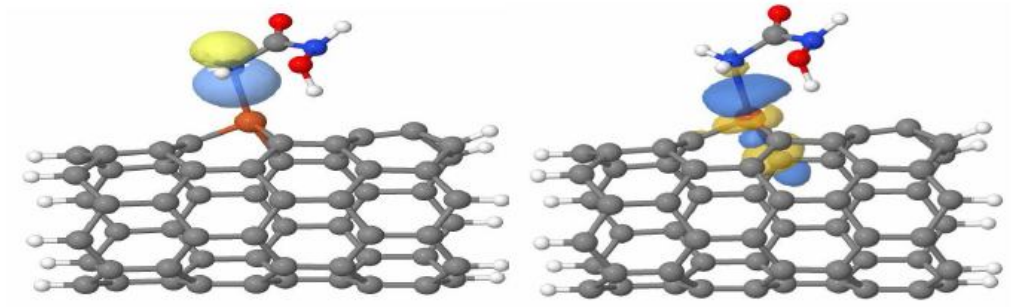

(D4) LP(1)N76 [HOMO]→ σ^*C50-Fe72: 42.98 kcal mol^{-1}

Fig. 8. Selected orbital interaction for doped complexes.

and shown in Fig. 5. The different interactions are represented by the color-filled $s(\rho)$ isosurfaces. Green isosurfaces show low electron density, corresponding to vdW interactions, blue color indicates the attractive interactions, and red color denotes strong repulsive interactions. The center of nanotubes and rings is specified by green isosurface confirming the vdW interaction (Fig. 6).

NBO Analysis

Natural bond orbital (NBO) calculations assort intra and inter charge transfers into the conjugations and hyper-conjugations. Stabilization energies owing to these charge transfers are obtained by the second order perturbation energy ($E^{(2)}$), that corresponds to the NBO interacting intensities. The most important Lewis and non-Lewis type NBOs and $E^{(2)}$ values are given in Table 5. Results show that donor orbitals of oxygen and nitrogen atoms of the drug (LP orbitals) transfer electrons to the acceptor orbitals of carbon nanotube (anti-bond orbitals of σ^* and π^*). The lone pairs of oxygen and nitrogen (LP_O, LP_N) take the major role in the charge transfer process. Although in the complex D2, both LP_O and LP_N participate but due to spatial orientation, LP_O plays an important role. The summation values of $E^{(2)}$ for D1 (37.61 kcal mol^{-1}), D2 (66.11 kcal mol^{-1}), D3 (68.9 kcal mol^{-1}) and D4 (47.1 kcal mol^{-1}) indicate that D3 and D1 have the highest and the lowest energy, respectively, which are in good agreement with the results of adsorption energies (Table 2). Briefly, the results of NBO analysis confirmed the interaction of NHU drug with Fe-doped and undoped complexes. Therefore, there is a charge transfer between SWCNT and the NHU molecule. Charges are moved from CNTs to the drug while in the case of the Fe-doped complex; the charges are transferred from the drug to the CNT. Figures 7 and 8. Present graphical figures of NBO interactions between HOMO and LUMO orbitals of complexes. As can be seen, there is a good overlap between NHU and nanotubes and orientation of the donor orbitals with higher value of $E^{(2)}$ energy is more suitable to interact with σ^* and π^* of acceptor atoms. It can also be seen that in doped complexes, HOMO (donor) and LUMO (acceptor) are located on the NHU and nanotube, respectively. In contrast to doped complexes, in undoped complexes the nanotube acts as a donor due to the large charge density over the nanotube. In brief, the results of NBO confirmed the interaction of drug molecule with the doped and undoped carbon nanotubes.

CONCLUSIONS

DFT calculations were performed to characterize the adsorption ability of N-hydroxyurea drug onto pristine and Fe-doped carbon nanotube. To consider the long-range interaction energy, CAM-B3LYP was also investigated. Data leading to this point long-range correction is so important to prevent some mistakes in results. The results show that Fe-doped CNT performs as a good adsorbent nanosystem compared to pristine CNT. Natural bond orbital analysis suggests that adsorption of drug onto undoped and doped nanotubes is different. In undoped complex, drug is an acceptor while in doped complexes drug acts as an electron donor. The NHU drug prefers to be adsorbed on the nanotubes *via* its -C=O and -NH2 groups for Fe-doped and undoped complexes, respectively. Results indicated that all of the complexes are stable in both phases especially in the aqueous phase. Finally, doping of CNTs with iron atom can increase the surface reactivity of nanotube towards the drug adsorption.

REFERENCES

[1] Angona, A.; Bellosillo, B.; Alvarez-Larrán, A.; Martínez-Avilés, L.; Camacho, L.; Pairet, S.; Fernández-Rodriguez, M. C.; Ancochea, À.; Besses, C. Genetic predisposition to molecular response in patients with myeloproliferative neoplasms treated with hydroxycarbamide. *Leuk. Res.,* **2013**, *37*, 917-921. DOI: 10.1016/j.leukres.

[2] Platt, O. S., Hydroxyurea for the treatment of sickle cell anemia. *N. Engl. J. Med.* **2008**, *358*, 1362-1369. DOI: 10.1056/NEJMct0708272.

[3] Liebelt, E. L.; Balk, S. J.; Faber, W.; Fisher, J. W.; Hughes, C. L.; Lanzkron, S. M.; Lewis, K. M.; Marchetti, F.; Mehendale, H. M.; Rogers, J. M., NTP-CERHR Expert Panel Report on the reproductive and developmental toxicity of hydroxyurea. *Res. Part B: Dev. Reprod. Toxicol,* **2007**, *80*, 259-366. DOI: 10.1002/bdrb.20123.

[4] Barbui, T.; Barosi, G.; Birgegard, G.; Cervantes, F.;

Finazzi, G.; Griesshammer, M.; Harrison, C.; Hasselbalch, H. C.; Hehlmann, R.; Hoffman, R., Philadelphia-negative classical myeloproliferative neoplasms: critical concepts and management recommendations from European Leukemia Net. *J. Clin. Oncol.,* **2011**, *29*, 761-770.

[5] Bertrand, N.; Leroux, J. -C.; The journey of a drug-carrier in the body: an anatomo-physiological perspective, *J. Control. Release,* **2012**, *161*, 152-163. DOI: 10.1016/j.jconrel.

[6] Bhirde, A. A.; Patel, V.; Gavard, J.; Zhang, G.; Sousa, A. A.; Masedunskas, A.; Leapman, R. D.; Weigert, R.; Gutkind, J. S.; Rusling, J. F., Targeted killing of cancer cells in vivo and in vitro with EGF-directed carbon nanotube-based drug delivery. *ACS Nano,* **2009**, *3*, 307-316. DOI: 10.1021/nn800551s

[7] Heister, E.; Neves, V.; Tîlmaciu, C.; Lipert, K.; Beltrán, V. S.; Coley, H. M.; Silva, S. R. P.; McFadden, J., Triple functionalisation of single-walled carbon nanotubes with doxorubicin, a monoclonal antibody, and a fluorescent marker for targeted cancer therapy. *Carbon,* **2009**, *47*, 2152-2160. DOI: 10.1016/j.carbon.

[8] Raju, H. B.; Goldberg, J. L., Nanotechnology for ocular therapeutics and tissue repair. *Expert Rev. Ophthalmol.,* **2008**, *3*, 431-436. DOI: 10.1586/17469899.3.4.431

[9] Foldvari, M.; Bagonluri, M., Carbon nanotubes as functional excipients for nanomedicines: II. Drug delivery and biocompatibility issues, Nanomed: Nanotechnol. *Biology and Med.,* **2008**, *4*, 183-200. DOI: 10.1016/j.nano.

[10] Zhao, X.; Liu, R., Recent progress and perspectives on the toxicity of carbon nanotubes at organism, organ, cell, and biomacromolecule levels. *Environ. Int.,* **2012**, *40*, 244-255. DOI: 10.1016/j.envint.

[11] Gomez-Gualdron, D. A.; Burgos, J. C.; Yu, J.; Balbuena, P. B., Carbon nanotubes: engineering biomedical applications. *Prog. Mol. Biol. Transl. Sci.,* **2010**, *104*, 175-245. DOI: 10.1016/B978-0-12-416020-0.00005-X.

[12] Liu, Z.; Sun, X.; Nakayama-Ratchford, N.; Dai, H., Supramolecular chemistry on water-soluble carbon nanotubes for drug loading and delivery. *ACS Nano,* **2007**, *1*, 50-56. DOI: 10.1021/nn700040t.

[13] Horie, M.; Stowe, M.; Tabei, M.; Kato, H.; Nakamura, A.; Endoh, S.; Morimoto, Y.; Fujita, K., Dispersant affects the cellular influences of single-wall carbon nanotube: the role of CNT as carrier of dispersants. *Toxicol. Mech. and Methods,* **2013**, *23*, 315-322. DOI: 10.3109/15376516.2012.755595.

[14] Mananghaya, M., Modeling of single-walled carbon nanotubes functionalized with carboxylic and amide groups towards its solubilization in water, *J. Mol. Liquids,* **2015**, *212*, 592-596. DOI: 10.1016/j.molliq.

[15] Mananghaya, M. R.; Santos, G. N.; Yu, D. N., Solubility of amide functionalized single wall carbon nanotubes: a quantum mechanical study, *J. Mol. Liquids,* **2017**, *242*, 1208-1214. DOI: 10.1016/j.molliq.

[16] Mananghaya, M.; Promentilla, M. A.; Aviso, K.; Tan, R., Theoretical investigation of the solubilization of cooh-functionalized single wall carbon nanotubes in water, *J. Mol. Liquids,* **2016**, *215*, 780-786. DOI: 10.1016/j.molliq.

[17] Koopmans, T., Über die Zuordnung von Wellenfunktionen und Eigenwerten zu den einzelnen Elektronen eines Atoms. *Physica,* **1934**, *1*, 104-113. DOI: 10.1016/S0031-8914(34)90011-2.

[18] Tsuneda, T.; Song, J. -W.; Suzuki, S.; Hirao, K., On Koopmans' theorem in density functional theory. *J. chem. Phys.,* **2010**, *133*, 174101. DOI: 10.1063/1.3491272.

[19] Becke, A. D., A new mixing of Hartree-Fock and local density-functional theories. *J. Chem. Phys.,* **1993**, *98*, 1372-1377. DOI: 10.1063/1.464304.

[20] Yanai, T.; Tew, D. P.; Handy, N. C., A new hybrid exchange-correlation functional using the Coulomb-attenuating method (CAM-B3LYP). *Chem. Phys. Lett.,* **2004**, *393*, 51-57. DOI: 10.1016/j.cplett.

[21] Kobayashi, R.; Amos, R. D., The application of CAM-B3LYP to the charge-transfer band problem of the zincbacteriochlorin–bacteriochlorin complex. *Chem. Phys. Lett.,* **2006**, *420*, 106-109. DOI: 10.1016/j.cplett.

[22] Frisch, M.; Trucks, G.; Schlegel, H.; Scuseria, G.; Robb, M.; Cheeseman, J.; Montgomery, J.; Vreven, T.; Kudin K.; Burant, J., Gaussian 09, Revision C. 02,

2008.

[23] Tomasi, J.; Mennucci, B.; Cammi, R., Quantum mechanical continuum solvation models. *Chem. Rev.,* **2005**, *105*, 2999-3094. DOI: 10.1021/cr9904009

[24] Boys, S.; Bernardi, F., The calculation of small molecular interactions by the differences of separate total energies. Some procedures with reduced errors. *Mol. Phys.,* **2002**, *100*, 65-73. DOI: 10.1080/00268977000101561.

[25] Parr, R. G.; Donnelly, R. A.; Levy, M.; Palke, W. E., Electronegativity: the density functional viewpoint. *J. Chem. Phys.,* **1978**, *68*, 3801-3807. DOI: 10.1063/1.436185.

[26] Parr, R. G.; Yang, W., Density functional approach to the frontier-electron theory of chemical reactivity. *J. Am. Chem. Soc.,* **1984**, *106*, 4049-4050.

[27] Biegler, K. F.; Schnbohm J.; Bayles, D., A Program to Analyze and Visualize Atoms in Molecules. 2001.

[28] Glendening, E. D.; Landis C. R.; Weinhold, F., NBO 6.0: natural bond orbital analysis program, *J. Comput. Chem.* **2013**, *34*, 1429-1437. DOI: 10.1002/jcc.23266

[29] Patek, M., Jmol NBO Visualization Helper Program, 2013.

[30] Okulik, N.; Jubert, A. H., Theoretical analysis of the reactive sites of non-steroidal anti-inflammatory drugs. *Internet. Electr. J. Mol. Des.* **2005**, *4*, 17-30.

[31] Parr, R. G.; Szentpaly, L.; Liu, S., Electrophilicity index. *J. Am. Chem. Soc.* **1999**, *121*, 1922-1924. DOI: 10.1021/ja983494x.

[32] Xiao, H.; Tahir-Kheli, J.; Goddard W. A., Accurate band gaps for semiconductors from density functional theory. *J. Phys. Chem. Lett.,* **2011**, *2*, 212-217. DOI: 10.1021/jz101565j.

[33] Matsuda, Y.; Tahir-Kheli, J.; Goddard W. A., Definitive band gaps for single-wall carbon nanotubes. *J. Phys. Chem. Lett.,* **2010**, *1*, 2946-2950. DOI: 10.1021/jz100889u.

[34] Becke, A.; Matta, C. F.; Boyd, R. J., The quantum theory of atoms in molecules: from solid state to DNA and drug design. John Wiley & Sons, 2007.

[35] Rozas, I.; Alkorta, I.; Elguero, J., Behavior of ylides containing N, O and C atoms as hydrogen bond acceptors. *J. Am. Chem. Soc.,* **2000**, *122*, 11154-11161. DOI: 10.1021/ja0017864.

[36] Ziółkowski, M.; Grabowski, S. J.; Leszczynski, J., Cooperativity in hydrogen-bonded interactions: ab initio and "atoms in molecules" analyses. *J. Phys. Chem. A,* **2006**, *110*, 6514.

[37] Lu, T.; Chen, F., Multiwfn: a multifunctional wavefunction analyzer, *J. Comput. Chem.,* **2012**, *33*, 580-592. DOI: 10.1021/jp060537k

[38] Humphrey, W.; Dalke, A.; Schulten, K., VMD: visual molecular dynamics. *J. Mol. Graph.,* **1996**, *14*, 33-38. DOI: 10.1016/0263-7855(96)00018-5.

[39] Johnson, E. R.; Keinan, S.; Mori-Sanchez, P.; Contreras-Garcia, J.; Cohen, A. J.; Yang, W., Revealing non-covalent interactions. *J. Am. Chem. Soc.,* **2010**, *132*, 6498. DOI: 10.1039/C2CP41395G.

[40] Contreras-Garcia, J.; Johnson, E. R.; Keinan, S.; Chaudret, R.; Piquemal, J. -P.; Beratan, D. N.; Yang, W., NCIPLOT: a program for plotting non-covalent interaction regions, *J. Chem. Theory. Comput.,* **2011**, *7*, 625-632. DOI: 10.1021/ct100641a.